

FedRTS: Federated Robust Pruning via Combinatorial Thompson Sampling

Hong Huang¹ Hai Yang¹ Yuan Chen¹ Jiaxun Ye¹ Dapeng Wu¹

Abstract

Federated Learning (FL) enables collaborative model training across distributed clients without data sharing, but its high computational and communication demands strain resource-constrained devices. While existing methods use dynamic pruning to improve efficiency by periodically adjusting sparse model topologies while maintaining sparsity, these approaches suffer from issues such as **greedy adjustments**, **unstable topologies**, and **communication inefficiency**, resulting in less robust models and suboptimal performance under data heterogeneity and partial client availability. To address these challenges, we propose **Federated Robust pruning via combinatorial Thompson Sampling (FedRTS)**, a novel framework designed to develop robust sparse models. FedRTS enhances robustness and performance through its Thompson Sampling-based Adjustment (TSAdj) mechanism, which uses probabilistic decisions informed by stable, farsighted information instead of deterministic decisions reliant on unstable and myopic information in previous methods. Extensive experiments demonstrate that FedRTS achieves state-of-the-art performance in computer vision and natural language processing tasks while reducing communication costs, particularly excelling in scenarios with heterogeneous data distributions and partial client participation. Our codes are available at: <https://github.com/Little0o0/FedRTS>.

1. Introduction

Federated learning (FL) (McMahan et al., 2017; Li et al., 2019; Kairouz et al., 2021) enables edge devices with private local data to collaboratively train a model without sharing

¹Department of Computer Science, City University of Hong Kong, Hong Kong SAR. Correspondence to: Hong Huang <honghuang2000@outlook.com>, Hai Yang <lyzs23333@gmail.com>, Yuan Chen <ychen2752-c@my.cityu.edu.hk>, Jiaxun Ye <jiaxunye@cityu.edu.hk>, Dapeng Wu <dpwu@ieee.org>.

Preliminary work.

data. However, substantial computational and communication demands for training deep learning models often exceed the resource limitations of edge devices in cross-device FL scenarios. Although neural network pruning (Han et al., 2015; Molchanov et al., 2019a; Ma et al., 2021) offers a promising solution by removing redundant parameters, traditional pruning methods depend on resource-intensive dense model training, rendering them impractical for privacy-preserved and resource-constrained FL environments.

To address these challenges, recent federated pruning frameworks (Bibikar et al., 2022; Qiu et al., 2022; Tian et al., 2024; Jiang et al., 2022; Huang et al., 2024; 2023; Munir et al., 2021) have adopted dynamic pruning techniques (Evci et al., 2020; Raihan & Aamodt, 2020; Jayakumar et al., 2020) within FL. These frameworks employ a two-loop training process: in the inner loop, model weights are updated through standard FL rounds with fixed model topology; in the outer loop, the server adjusts the model topology by pruning and reactivating parameters (Evci et al., 2020), as illustrated in Fig. 1 (left). This iterative process generates a specialized sparse model without dense model training, significantly reducing computational costs.

Despite these advancements, existing frameworks suffer from three critical challenges in model topology adjustment (Bibikar et al., 2022; Qiu et al., 2022; Tian et al., 2024; Jiang et al., 2022; Huang et al., 2024; 2023; Munir et al., 2021), as illustrated in Fig. 1 (left). **1). Greedy adjustment:** Current methods rely on myopic, aggregated information from a small subset of participating clients, ignoring data from the majority of unseen clients and prior knowledge. This leads to greedy adjustments and reduced robustness (Kairouz et al., 2021). **2). Unstable topology:** Deterministic adjustments based solely on aggregated information are prone to instability due to heterogeneous data distributions, resulting in unstable model topologies. **3). Communication inefficiency:** Transmitting extensive auxiliary data (e.g., full gradient matrices) for topology updates imposes high communication costs. These limitations hinder the ability of current methods to handle client availability, data heterogeneity, and communication costs effectively, ultimately leading to suboptimal performance and inefficient resource utilization.

To address these challenges, *we reframe federated prun-*

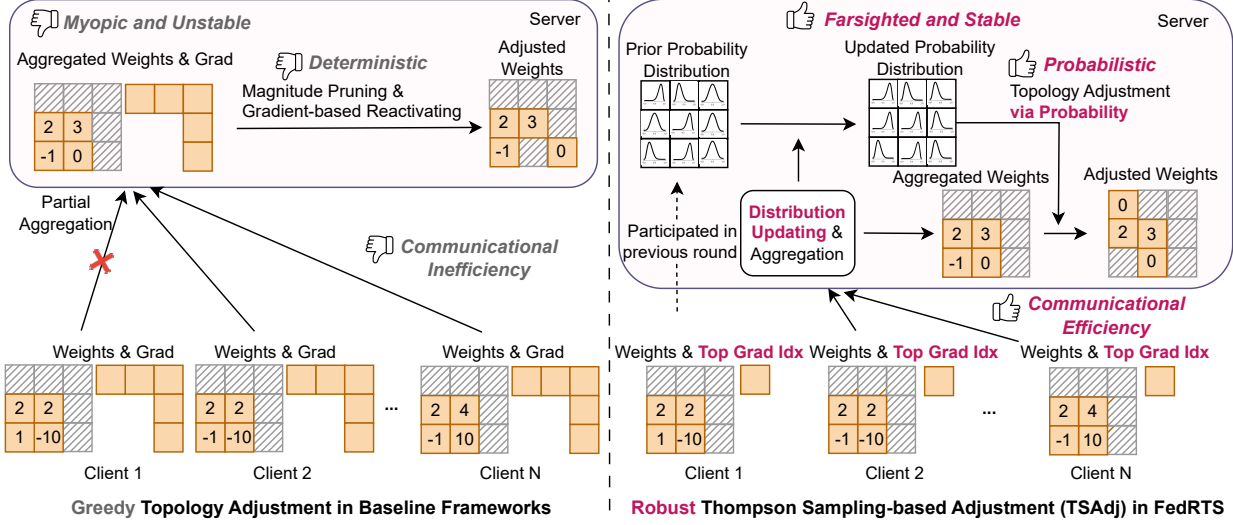


Figure 1. Illustration of topology adjustment in existing baselines and FedRTS. *Left*: Existing baselines adjust model topology based on myopic and unstable aggregated weights and gradients via deterministic magnitude pruning and reactivating, resulting in greedy adjustment and high communication overhead. *Right*: FedRTS introduces Thompson Sampling-based Adjustment (TSAdj) to adjust the topology based on farsighted and stable prior probability distributions, achieving a robust topology and low communication overhead.

ing as a combinatorial multi-armed bandit (CMAB) (Chen et al., 2013) problem and identify the above issues located in myopic observation and deterministic decision. Building on this insight, we propose **Federated Robust** pruning via combinatorial **Thompson Sampling** (FedRTS), a novel framework designed to derive robust sparse models for cross-device FL, as illustrated in Fig. 2. FedRTS introduces the Thompson Sampling-based Adjustment (TSAdj) mechanism, depicted in Fig. 1 (right), to address the shortcomings of existing methods. First, TSAdj leverages farsighted probability distributions (including prior information from unseen clients) to mitigate the impact of partial client participation. Second, it uses probabilistic decisions based on stable, comprehensive information rather than deterministic adjustments from unstable aggregated information. Third, FedRTS reduces communication overhead by requiring clients to upload only top-gradient indices for adjustments.

We evaluate FedRTS on computer vision and natural language processing datasets, demonstrating its effectiveness in handling client availability and data heterogeneity. FedRTS achieves higher accuracy, better generalization, and lower communication costs compared to state-of-the-art (SOTA) methods. For instance, on the CIFAR-10 dataset with the ResNet-18 model, FedRTS achieves either a 5.1% accuracy improvement or a 33.3% reduction in communication costs compared to SOTA frameworks. *To our knowledge, this paper is the first work to analyze federated pruning through a CMAB lens and apply combinatorial Thompson sampling to stabilize topology adjustments in FL.*

2. Preliminary and Challenges

2.1. Federated Dynamic Pruning

In federated pruning, \mathcal{N} resource-constrained clients collaboratively train a sparse model using their local datasets $D_n, n \in \{1, 2, \dots, \mathcal{N}\}$. Given the target density d' , the objective is to solve the following optimization problem:

$$\min_{W, m} \sum_{n=1}^{\mathcal{N}} p_n f_n(W, m, D_n), \quad \text{s.t. } d \leq d', \quad (1)$$

where W represents the model weights, $m \in \{0, 1\}^{\langle W \rangle}$ denotes the sparse model topology (also called mask), $f_n(\cdot)$ is the objective function for client n , d is the density of the topology m , and p_n is set as the proportion of the dataset size of client n , typically set as $p_n = \langle D_n \rangle / \sum_{i=1}^{\mathcal{N}} \langle D_i \rangle$.¹

To solve the problem in Eq. 1 under the target density constraint d' , existing federated pruning frameworks (Bibikar et al., 2022; Qiu et al., 2022; Tian et al., 2024; Jiang et al., 2022; Huang et al., 2024; 2023; Munir et al., 2021) apply dynamic pruning techniques (Evci et al., 2020; Raihan & Aamodt, 2020; Jayakumar et al., 2020) within FL. These frameworks iteratively adjust sparse on-device models during training while maintaining the density level d . The process begins with a sparse model initialized via random pruning and follows a two-loop training procedure: In the inner loop, the model topology m remains fixed, and the model weights are updated through traditional FL rounds. After ΔT inner loops, as illustrated in Fig. 1 (left), the framework enters the outer loop, where clients upload additional data (specifically, the gradients of the pruned weights)

¹In this paper, $\langle \cdot \rangle$ is the cardinal number of the set.

to the server. The server then adjusts the model topology by pruning and reactivating (Evci et al., 2020) based on the aggregated weights and gradients.

2.2. CMAB-Based Problem Formulation

The Combinatorial Multi-Armed Bandit (CMAB) (Chen et al., 2013; Slivkins et al., 2019; Kong et al., 2021) is a sequential decision-making framework where an agent selects combinations of arms (called super arms) with unknown reward distributions. The objective is to maximize cumulative rewards by balancing the exploration of uncertain arms and the exploitation of high-performing ones.

We formulate the topology adjustment as a CMAB problem, where each link m_i in the model topology serves as an arm. In each outer loop t for topology adjustment, the server selects an action S_t , which includes K arms, where $K = d'\langle W \rangle$. Selected arms $i \in S_t$ are activated ($m_{t,i} = 1$), while others $i \notin S_t$ are deactivated ($m_{t,i} = 0$). After playing action, the new sparse weights $W_t = W_t^{agg} \odot m_t$ will be distributed to the clients for further training, where W_t^{agg} is the aggregated weights. The server then observes outcomes $X_t = (X_{t,1}, \dots, X_{t,m})$, drawn from distributions with unknown expectation μ . After that, the server obtains the unknown rewards $R_t = R(S_t, X_t)$. At the next round $t + 1$, the previous information $\{X_\tau | 1 \leq \tau \leq t\}$ is the input to the adjustment algorithm to select the action S_{t+1} . Following previous work (Kong et al., 2021), we assume that the expected reward of an action S_t only depends on S_t and the mean vector μ , i.e., there exists a function r such that $\mathbb{E}[R_t] = \mathbb{E}_{X_t}[R(S_t, X_t)] = r(S_t, \mu)$.

2.3. Challenges in Previous Methods

From the CMAB aspect, after taking the action S_t , previous federated pruning methods observe the delay outcomes X_t at the next outer loop $t + 1$, where $X_{t,i} = 1$ if i is the index of the top magnitude of aggregated weights $|W_{t+1}^{agg}|$ or gradients $|G_{t+1}^{agg}|$; otherwise, $X_{t,i} = 0$. Treating the outcomes $\{X_t\}$ as the feedback, the next action S_{t+1} is selected, i.e., $S_{t+1} = \{i | X_{t,i} = 1\}$. Thereby these methods face three significant challenges:

Greedy Adjustment: Existing frameworks only observe the outcomes in the outer loop, ignoring the inner loop. Moreover, they discard all previous information $\{X_\tau | 1 \leq \tau \leq t - 1\}$, which is myopic, excluding information from unseen clients and previous data, leading to a greedy topology adjustment that is difficult to exploit from a global view.

Unstable Topology: Previous ignore the expectation of distribution μ and make a deterministic decision based on unreliable outcomes X_t . It is hard to maximize the reward expectation $r(S_t, \mu)$ and may select an arm with a low expectation, leading to an unstable topology.

Communication Inefficiency: Existing frameworks require clients to upload gradients for pruned weights during topology adjustments, making the total communication cost equivalent to that of a dense model, thus lacking communication efficiency. Although some approaches try to mitigate this by uploading only the top gradients (Huang et al., 2023; 2024) or placing adjustments on the client side (Bibikar et al., 2022; Tian et al., 2024), these methods make the adjustment more unstable, leading to suboptimal performance.

3. Methodology

In this section, we present FedRTS, a novel federated pruning framework designed to develop robust model topologies, as illustrated in Fig. 2. We begin by detailing the TSAdj mechanism, which serves as the core component for searching robust sparse topologies. Next, we provide an overview of the FedRTS algorithm that integrates TSAdj. Finally, we provide the theoretical regret upper bound of TSAdj.

3.1. Thompson Sampling-based Adjustment

We find that the core source of the aforementioned challenges in existing federated dynamic pruning frameworks lies in deterministic decision strategies and myopic observations. Therefore, we propose the Thompson Sampling based Adjustment (TSAdj) mechanism, which includes probabilistic decision strategy and farsighted observations. Moreover, TSAdj effectively reduces the communication overhead.

Compared to directly using myopic outcomes to make deterministic decisions, our proposed TSAdj maintains individual prior probability distributions P for each link in the model topology m during training. The higher feedback a link i has gained from previous observations, the closer the expectation of its probability $E[P_i]$ approaches 1, indicating a higher likelihood of being selected. In the outer loop for topology adjustment, instead of deterministically selection based on outcomes X_t , the server samples random variables $\xi \sim P$ and selects an action S_t on the topology as follows:

$$S_t = \{i | \xi_i \in \text{Top}(\xi, K)\}, \quad (2)$$

where $\text{Top}(\xi, K)$ denotes the set of top K elements of ξ . The action S_t is derived from the expectation of the prior distribution, $E[P]$, which provides a more stable topology compared to existing approaches.

Unlike existing approaches that develop the outcomes using immediate and myopic data in the outer loop, TSAdj derives much more comprehensive outcomes X_t from both the inner and outer loops. After performing action S_t , the outcome X_t is observed in the end of loop t , and is formulated as a combination of individual outcomes X_t^n and aggregated

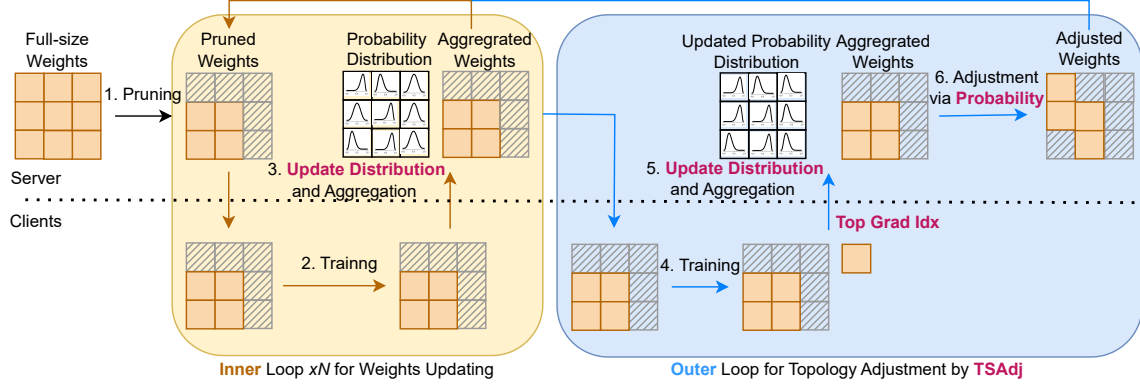


Figure 2. The overview of the FedRTS, which integrates TSAdj and utilizes the two-loop updating to develop a robust sparse model.

outcomes X_t^{agg} :

$$X_t = (1 - \gamma)X_t^{agg} + \gamma \sum_{n \in C_t} p_n X_t^n, \quad (3)$$

where γ is the trade-off ratio, C_t is the set of clients that participate FL in loop t . This fusion mechanism mitigates biases that arise from unstable aggregated data.

We consider the semi-outcomes for X_t^{agg} and X_t^n in the inner loop, *i.e.*, only the arms $i \in S_t$ have the outcomes. We define a constant $\kappa < K$, which denotes the number of core links (arms) in the model topology, and during the adjustment, we expect that $K - \kappa$ less important links are pruned, while $K - \kappa$ candidate links are reactivated. Therefore, when the loop $t + 1$ is the inner loop, we have

$$X_{t,i}^{agg} = h(i, |W_{t+1}^{agg}|, \kappa), \quad i \in S_t, \quad (4)$$

$$X_{t,i}^n = h(i, |W_{t+1}^n|, \kappa), \quad i \in S_t, \quad (5)$$

where W_{t+1}^{agg} and W_{t+1}^n represent the aggregated weights and client n 's weights, respectively, and $h(\cdot)$ is a discriminative function defined as $h(i, x, \kappa) = \mathbf{1}_{i \in \text{Top}(x, \kappa)}$. In the inner loop, for arms $i \notin S_t$, both the aggregated outcomes $X_{t,i}^{agg}$ and the individual outcomes $X_{t,i}^n$ are set to *None*. In the outer loop, we consider the full outcomes of X_t^{agg} and X_t^n as the gradients for inactivated weights are available. For the arms $i \notin S_t$, the individual outcomes $X_{t,i}^n$ are defined as

$$X_{t,i}^n = h(i, |G_{t+1}^n|, K - \kappa), \quad i \notin S_t, \quad (6)$$

where the G_{t+1}^n denotes the gradients of the weights W_{t+1}^n . Here, $K - \kappa$ is used to treat some inactivated arms as candidates for reactivation. We set the aggregated outcomes $X_{t,i}^{agg} = 0.5$ for $i \notin S_t$ in the outer loop, without using the aggregated gradients G_{t+1}^{agg} due to their high variance. Notably, the clients only upload the Top $K - \kappa$ indices of gradients magnitude $|G_{t+1}^n|$ to achieve 6, rather than the

full gradients, significantly reducing the communication overhead.

To construct a posterior probability distribution, TSAdj updates the prior distribution P based on outcomes X_t . Following the Thompson Sampling framework, each P_i is modeled as a Beta distribution with factors α_i, β_i , representing the likelihood of selecting an arm into S_t : a higher α_i shifts $\mathbb{E}[P_i]$ towards 1, whereas a higher β_i shifts it towards 0. The (α_i, β_i) are updated via Bayes' rule, leveraging its conjugacy properties and using the outcomes $X_{t,i}$ as follows:

$$(\alpha_i, \beta_i) \leftarrow (\alpha_i + \lambda X_{t,i}, \beta_i + \lambda(1 - X_{t,i})), \quad X_{t,i} \neq \text{None}, \quad (7)$$

where λ is a scaling factor that determines the influence of outcomes. Over time, the distribution gradually converges towards the true distribution, aligning with the observed outcomes. The overflow of TSAdj is shown in Algorithm 1.

Algorithm 1 TSAdj

Input: Uploaded sparse weights $\{W_{t+1}^n\}_{n \in C_t}$ and gradients $\{G_{t+1}^n\}_{n \in C_t}$, global distribution factors (α, β) .

Output: Updated weights W_{t+1} and topology m_{t+1}

$W_{t+1}^{agg} \leftarrow \sum_{n \in C_t} p_n W_{t+1}^n$

$X_t^{agg} \leftarrow$ calculate by Eq.4 based on W_{t+1}^{agg}

$X_t^n \leftarrow$ calculate by Eq.5,6 based on W_{t+1}^n and G_{t+1}^n

$X_t \leftarrow (1 - \gamma)X_t^{agg} + \gamma \sum_{n \in C_{t+1}} p_n X_t^n$

$(\alpha_i, \beta_i) \leftarrow (\alpha_i + \lambda X_{t,i}, \beta_i + \lambda(1 - X_{t,i})), X_{t,i} \neq \text{None}$

$\xi \leftarrow$ sample from $\text{Beta}(\alpha, \beta)$

$S_t \leftarrow \{i | \xi_i \in \text{Top}(\xi, K)\}$

$m_{t+1} \leftarrow$ adjust m_t based on action S_t

$W_{t+1} \leftarrow W_{t+1}^{agg} \odot m_{t+1}$

In summary, TSAdj leverages the prior probability distributions P to probabilistically guide topology adjustments and uses comprehensive outcomes X_t to update the distributions, which mitigates instability caused by myopic adjustments, enabling smoother convergence and developing a more reliable topology. Moreover, TSAdj requires the clients to

upload only the most critical gradient information, thereby reducing the communication overhead.

3.2. FedRTS

FedRTS is a novel federated learning framework designed to address the limitations of existing dynamic sparse training methods by integrating the Thompson Sampling-based Adjustment (TSAdj) mechanism, as illustrated in Fig. 2. The framework begins with an initialized model weight and sparse topology sampled from Beta distributions P . FedRTS employs a two-loop training process to iteratively update model weights and refine the sparse topology.

In the inner loop, the model topology remains fixed while the server updates the model weights and distribution P based on semi-outcomes. In the outer loop, the server collects the full outcomes by requiring clients to upload the top- κ gradient indices of inactivated weights. Using this information, the server applies TSAdj to make robust topology adjustments, and the updated topology is then distributed to clients. FedRTS continues this iterative process until model convergence. The details of FedRTS are shown in Algo. 2 and Sec. B.2.

By integrating TSAdj, FedRTS introduces a novel approach to sparse topology adjustment. Leveraging Thompson Sampling, it mitigates the instability caused by unstable aggressive topology, ensuring smoother convergence through probabilistically guided adjustments based on historical information. This adaptive adjustment strategy enhances the robustness of the sparse topology and improves overall model performance in FL tasks.

3.3. Theoretical Analysis

For simplifications, we omit the inter loop of FedRTS to isolate the TSAdj mechanism and consider only semi-outcomes, i.e., ignore the outcomes $X_{t,i}$ that $i \notin S_t$. We also consider the following assumption and approximation:

Assumption 3.1. (*Independent Magnitude*) *Magnitude of model weights are mutually independent.*

Assumption 3.2. (*Threshold Approximation*) *The discriminative function $h(\cdot)$ in Eq. 4 and 5 can be approximated by a threshold σ , i.e., $h(i, x, \kappa) \approx \mathbf{1}_{x \geq \sigma}$.*

Assumption 3.1 aligns with standard magnitude pruning practices, while Assumption 3.2 holds empirically, as weights often exhibit a Gaussian-like distribution under L2 regularization and normalization techniques. Therefore, under assumptions 3.1 and 3.2, the outcomes $X_{t,i}$ become:

$$X_{t,i} = \gamma \mathbf{1}_{|W_{t,i}| \geq \sigma} + (1 - \gamma) \sum_n p_n \mathbf{1}_{|W_{t,i}^n| \geq \sigma}, \quad i \in S_t, \quad (8)$$

which are mutually independent. We also include the Lipschitz assumption 3.3 as in previous work (Kong et al., 2021).

Assumption 3.3. (*Lipschitz continuity*) $\exists L \in \mathbb{R}, \forall S, \mu, \mu'$ satisfies $|r(S, \mu) - r(S, \mu')| \leq L \|\mu - \mu'\|_1$.

The cumulative regret $Reg(T)$ is defined as:

$$Reg(T) = \mathbb{E} \left[\sum_{t=1}^T \Delta_{S_t} \right], \quad (9)$$

where $\Delta_{S_t} = \max\{r(S^*, \mu) - r(S_t, \mu), 0\}$ and S^* is the greedy optimal action based on μ , which is obtained by Algo. 3. The maximum reward gap is set as $\Delta_{\max} = \max_S \Delta_S$. The maximum reward gap of actions containing arm s is $\Delta_s^{\max} = \max_{S: s \in S} \Delta_S$. We define S^* and S_t are sequences, i.e., $S^* = (s_1^*, \dots, s_K^*)$, $S_t = (s_{t,1}, \dots, s_{t,K})$, and $s_k^* \in S^*$ is the k -th element added to S^* . We denote $S_k^* = (s_1^*, \dots, s_k^*)$ and $S_{t,k} = (s_{t,1}, \dots, s_{t,k})$. For any arm s , define the marginal reward gap $\Delta_{s,k} = r(S_k^*, \mu) - r(S_{k-1}^* \cup \{s\}, \mu)$.

Inspired by previous work in combinatorial Thompson sampling (Chen et al., 2013; Kong et al., 2021), we provide a regret upper bound for TSAdj.

Theorem 3.4. (*Upper Bound*) *Under assumptions 3.1, 3.2 and 3.3 and with outcomes X_t defined in Eq. 8, the regret $Reg(T)$ of TSAdj can be upper bounded by:*

$$\begin{aligned} Reg(T) &\leq \sum_{s \neq s_1^*} \max_{k: s \notin S_k^*} \frac{6\Delta_s^{\max} L^2 \log T}{(\Delta_{s,k} - 2BK\epsilon)^2} \\ &\quad + \left(2K + 4\langle W \rangle + \frac{KU + 8K\epsilon^4}{\epsilon^6} \right) \Delta_{\max} \quad (10) \\ &= O \left(\sum_{s \neq s_1^*} \max_{k: s \notin S_k^*} \frac{\Delta_{\max} L^2 \log T}{\Delta_{s,k}^2} \right). \end{aligned}$$

for any ϵ such that $\forall s \neq s_1^*$ and $s \notin S_k^*, \Delta_{s,k} > 2BK\epsilon$, where U is a universal constant.

The proof detail is provided in Sec. C.2.

4. Evaluation

To validate the efficacy of FedRTS, we conduct comprehensive experiments in this section. Notably, we evaluate each experiment five times, reporting the mean results along with the standard errors. In the figures, the shaded area represents the standard errors. In the table, the best results are highlighted in **purple**, while the second-best results are marked in **orange**.

4.1. Experiment Setup

We provide a brief overview of the experimental setup in this section, with additional details in Appendix D.

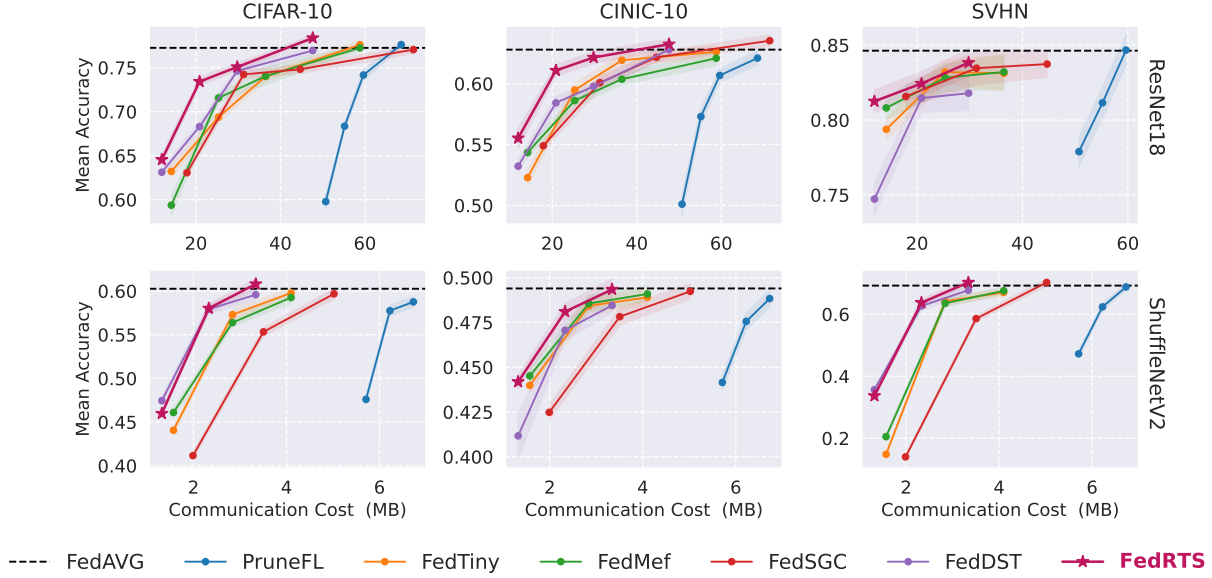


Figure 3. Testing accuracy of FedRTS and different federated pruning baselines on the three CV datasets with different densities.

Datasets and Models. Following previous work (Huang et al., 2023; 2024; Bibikar et al., 2022; Jiang et al., 2022) on federated dynamic pruning, we conduct experiments on CV tasks using two lightweight models, ResNet18 (He et al., 2016) and ShuffleNetV2 (Zhang et al., 2018), across three well-known image classification datasets: CIFAR-10 (Krizhevsky et al., 2009), CINIC-10 (Darlow et al., 2018), and SVHN (Netzer et al., 2011). For NLP tasks, we use the GPT-2-32M model on the TinyStories dataset (Eldan & Li, 2023), a language understanding benchmark designed for small language models.

Federated Learning Settings. Following the settings used in previous frameworks (Huang et al., 2023; 2024; Bibikar et al., 2022), we conduct 500 communication rounds with 5 local training epochs. Batch sizes are set to 64 for CV tasks and 16 for NLP tasks. In each round, 10 clients are randomly selected from a total of $N = 100$ clients. We perform an outer loop for topology adjustment every $\Delta T = 10$ inner loops until the total number of loops t reaches $T_{end} = 300$.

Baseline Settings. We select the following SOTA federated pruning frameworks as baselines: PruneFL (Jiang et al., 2022), FedTiny (Huang et al., 2023), FedDST (Bibikar et al., 2022), FedSGC (Tian et al., 2024), and FedMef (Huang et al., 2024). These methods incorporate dynamic pruning in FL and achieve SOTA performance across various settings. We adopt all hyperparameters specified in the original papers, except for those mentioned in the previous section. Additionally, some modules are disabled due to high resource demands, such as adaptive batch normalization selection in FedTiny, as detailed in Appendix D.3.

Implementation Details. Following previous work (Huang et al., 2023; 2024), we exclude bias terms, normalization

Target Density	Method	PPL ↓	Avg. Acc ↑	Comm. Cost ↓
1	FedAVG	20.56	0.4387	260.41MB
50%	FedDST	20.10	0.4261	138.30 MB
	FedSGC	26.13	0.4110	207.45 MB
	FedMef	20.61	0.4352	165.96 MB
	FedRTS	18.54	0.4422	138.84 MB
30%	FedDST	24.46	0.4263	86.26 MB
	FedSGC	32.39	0.3939	129.39 MB
	FedMef	21.00	0.4304	103.51 MB
	FedRTS	18.56	0.4405	86.44 MB
20%	FedDST	26.49	0.4219	60.22 MB
	FedSGC	43.00	0.3550	90.33 MB
	FedMef	21.53	0.4293	72.26 MB
	FedRTS	19.93	0.4333	60.34 MB

Table 1. Performance comparison on TinyStories with GPT-2-32M

layers, and the output layer from pruning while ensuring the overall density $d \leq d'$. Layer-wise sparsity follows the Erdos-Renyi-Kernel distribution (Evcı et al., 2020). We set the scaling factor $\lambda = 10$ and trade-off ratio $\gamma = 0.5$ as default, with their impacts analyzed in Sec. E.1 and E.2. Training FLOPs and communication costs are calculated as described in Sec. F.

4.2. Performance Evaluation

To demonstrate the effectiveness of FedRTS, we conduct experiments on both computer vision (CV) and neural language (NLP) tasks under various target density levels, reporting performance and communication costs for adjustment.

Computer Vision Tasks. In the CV tasks, we conduct experiments using the ResNet18 and ShuffleNetV2 models,

testing four target density levels: 50%, 30%, 20%, and 10% on CIFAR-10, CINIC-10, and SVHN datasets, reporting the accuracy and communication costs per outer loop. In some cases, FedRTS achieves similar accuracy to FedAVG at the 30% density ratio; therefore, results for the 50% density ratio are omitted. As shown in Fig. 3, FedRTS consistently outperforms all baseline methods in most scenarios in terms of both accuracy and communication efficiency. For instance, in the experiment with ResNet18 in CIFAR-10, FedRTS achieves a 5.1% improvement in accuracy over the best baseline methods while maintaining a similar communication cost (20MB). These gains are attributed to the robust adjustment, stable topology, and communication efficiency provided by TSAj in FedRTS.

An evident trend is the superior accuracy achieved by ResNet18 compared to ShuffleNetV2, due to ResNet18’s larger parameter space and higher representational capacity. Furthermore, FedDST and FedMef consistently outperform other baseline methods. Based on these empirical observations, we select ResNet18 as the default CV model and identify FedDST and FedMef as the primary reference for subsequent experiments.

Natural Language Processing Tasks. To evaluate the effectiveness of FedRTS across different domains, we conduct experiments on NLP tasks using the TinyStories dataset with the GPT-2-32M model. We test three target density levels: 50%, 30%, and 20%. Perplexity (PPL), which assesses model performance by considering the entire probability distribution in generated text, serves as the primary evaluation metric. As shown in Tab. 1, FedRTS outperforms all baselines, demonstrating its superiority in the NLP domain. Notably, FedRTS achieves better performance in perplexity than in accuracy-based evaluations, even surpassing full-size FedAVG at low-density levels. This improvement may stem from its probabilistic adjustment strategy, which enhances flexibility and adaptability during optimization. Unlike deterministic approaches, probabilistic adjustment enables FedRTS to prioritize critical parameters effectively, improving its ability to adapt to complex probability distributions. This is particularly beneficial for NLP tasks, where capturing intricate text patterns is essential, leading to lower perplexity scores and stronger performance in low-resource settings.

4.3. Robustness Analysis

To demonstrate the robustness of FedRTS in the face of heterogeneous data distributions and partial client participation, we conduct experiments with different degrees of data heterogeneity and client availability in this section.

The Impact of Data Heterogeneity. Data heterogeneity, or non-independent and identically distributed (non-IID) data, is a critical factor affecting performance in FL. To

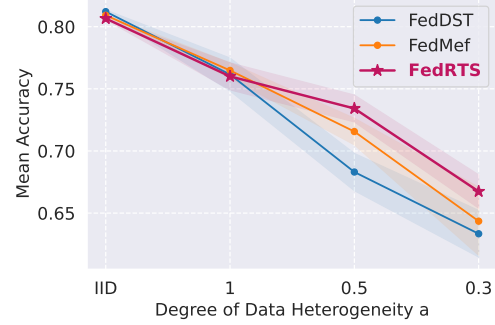


Figure 4. Accuracy on CIFAR-10 under various degrees of data heterogeneity. The lower a represents a higher non-IID degree.

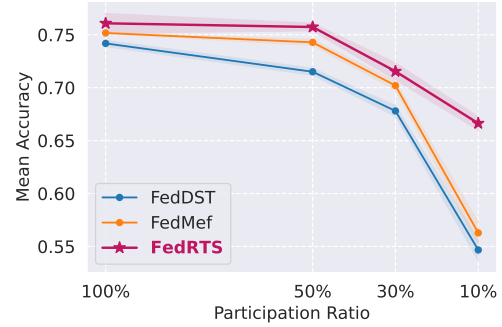


Figure 5. Accuracy on CIFAR-10 with various participation ratios of clients

demonstrate the robustness of FedRTS, we conduct experiments with varying degrees of data heterogeneity. By adjusting the Dirichlet distribution factor a across settings $\{0.3, 0.5, 1.0, IID\}$, we control the degree of data heterogeneity, where lower a indicates higher heterogeneity. As shown in Fig. 4, FedRTS outperforms all baselines, particularly in highly heterogeneous settings, demonstrating its effectiveness in handling non-IID data. This improvement is primarily attributed to the stable topology maintained by TSAj in FedRTS.

The Impact of Client Availability Client availability is another significant challenge in FL. To evaluate the robustness of FedRTS under different levels of client availability, we conduct experiments with participation ratios of 100%, 50%, 30%, 10% using a total of 10 clients. To mitigate slow convergence at lower participation levels, we adopt a high learning rate of 1 with SGD, as Adam exhibited instability with NaN values in our experiments. As shown in Fig. 5, FedRTS consistently outperforms all baselines, particularly at low participation ratios, demonstrating its adaptability and robustness in limited-client scenarios.

4.4. Ablation Study

To analyze the individual contributions of FedRTS in addressing greedy and unstable topology adjustment problems,

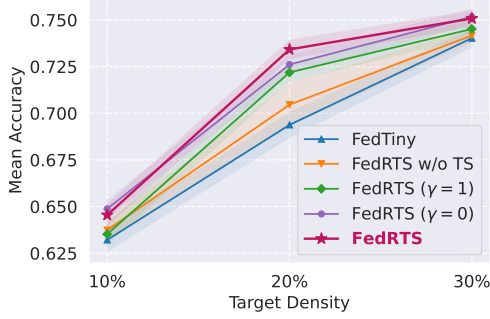


Figure 6. Accuracy on CIFAR-10 for FedRST and various variants.

we conduct an ablation study on the CIFAR-10 dataset with various target density levels. We consider the benefits of FedRTS to come from three aspects: probabilistic adjustment, stability, and farsighted information. To evaluate these aspects independently, we consider the following variants of FedRTS: 1) *FedRTS* ($\gamma = 0$): This variant does not use the aggregated information to update the probability distribution. 2) *FedRTS* ($\gamma = 1$): This variant only uses the aggregated information to update the probability distribution, which reduces stability. 3) *FedRTS without TS*: This variant fuses historical information via a momentum mechanism similar to FedAdam (Reddi et al., 2020) and uses deterministic adjustment to obtain the new topology instead of probabilistic adjustment. 4) *FedTiny*: This serves as a baseline to evaluate the overall effectiveness of FedRTS. The results in Figure 6 demonstrate the effectiveness of FedRTS. First, the performance of *FedRTS* and *FedRTS* ($\gamma = 0$) is similar but better than *FedRTS* ($\gamma = 1$), demonstrating that aggregated information suffers from instability. Including individual information can make the adjusted topology more stable and achieve better performance. Second, without deterministic adjustment, *FedRTS w/o TS* performs much worse than *FedRTS*, indicating the benefits of probabilistic adjustment. Third, *FedRTS w/o TS* is better than *FedTiny*, demonstrating the effectiveness of farsighted information. Therefore, the ablation study demonstrates the effectiveness of FedRTS in terms of probabilistic adjustment, stability, and farsighted information.

4.5. Efficiency Analysis

Training Cost. We evaluate FedRTS’s efficiency by analyzing training costs on CIFAR-10 and CINIC-10. To compare expenses, we measure total training FLOPs and communication costs required to match the testing accuracy of dense FedAVG. The accuracy is averaged over 10 rounds to mitigate variance from random factors, ensuring a more stable evaluation. As shown in Tab. 2, FedRTS achieves the testing accuracy of dense FedAVG with significantly lower costs. On CINIC-10, it achieves 48% training FLOPs and the communication cost compared to the best baseline

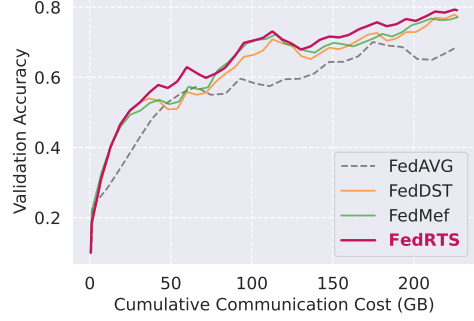


Figure 7. Validation accuracy of FedRTS and SOTA frameworks on CIFAR-10 dataset for cumulative communicational cost.

	CIFAR-10		CINIC-10	
	FLOPs	Comm. Cost	FLOPs	Comm. Cost
FedDST	3.4E16	221.9 GB	8.2E16	290.7 GB
FedMef	3.5E16	227.6 GB	6.1E16	222.3 GB
FedRTS	3.1E16	204.2 GB	2.9E16	105.6 GB

Table 2. The overall training FLOPs and communicational cost (Comm. Cost) for FedRTS and other frameworks to reach the testing accuracy of the dense FedAVG.

FedMef, which highlights the efficiency of FedRTS.

Convergence Behavior. Convergence is crucial for effective learning, precise predictions, and optimized resource use. To evaluate this, we track the validation accuracy of FedRTS and SOTA frameworks on CIFAR-10 against cumulative communication and computational costs, as shown in Fig. 7 and Sec. E.4. Accuracy is averaged over 10 rounds to reduce variance and provide a stable representation. Results show that FedRTS converges faster than other methods, achieving higher final accuracy with improved communication efficiency, highlighting the benefits of TSAdj in FedRTS in enhancing convergence.

5. Conclusion

In this paper, we analyze federated pruning from the perspective of combinatorial multi-armed bandits and identify key limitations in existing methods, including greedy adjustments, unstable topologies, and communication inefficiencies. To address these challenges, we propose Federated Robust Pruning via Combinatorial Thompson Sampling (FedRTS), a novel framework for developing robust sparse models. The core component of FedRTS, the Thompson Sampling-based Adjustment (TSAdj) module, enhances robustness and performance by making probabilistic decisions based on stable, farsighted information rather than deterministic decisions driven by unstable, myopic observations. We provide a theoretical regret upper bound for TSAdj and conduct extensive experiments, demonstrating that FedRTS achieves state-of-the-art performance in both computer vision and natural language processing tasks.

Impact Statement

This paper presents work whose goal is to advance the field of Machine Learning. There are many potential societal consequences of our work, none which we feel must be specifically highlighted here.

References

- Bibikar, S., Vikalo, H., Wang, Z., and Chen, X. Federated dynamic sparse training: Computing less, communicating less, yet learning better. In *Proceedings of the AAAI Conference on Artificial Intelligence*, volume 36, pp. 6080–6088, 2022.
- Chen, W., Wang, Y., and Yuan, Y. Combinatorial multi-armed bandit: General framework and applications. In *International conference on machine learning*, pp. 151–159. PMLR, 2013.
- Chen, W., Wang, Y., Yuan, Y., and Wang, Q. Combinatorial multi-armed bandit and its extension to probabilistically triggered arms. *Journal of Machine Learning Research*, 17(50):1–33, 2016.
- Darlow, L. N., Crowley, E. J., Antoniou, A., and Storkey, A. J. Cinic-10 is not imagenet or cifar-10. *arXiv preprint arXiv:1810.03505*, 2018.
- Dettmers, T. and Zettlemoyer, L. Sparse networks from scratch: Faster training without losing performance. *arXiv preprint arXiv:1907.04840*, 2019.
- Eldan, R. and Li, Y. Tinstories: How small can language models be and still speak coherent english? *arXiv preprint arXiv:2305.07759*, 2023.
- Evci, U., Gale, T., Menick, J., Castro, P. S., and Elsen, E. Rigging the lottery: Making all tickets winners. In *International Conference on Machine Learning*, pp. 2943–2952. PMLR, 2020.
- Gai, Y., Krishnamachari, B., and Jain, R. Combinatorial network optimization with unknown variables: Multi-armed bandits with linear rewards and individual observations. *IEEE/ACM Transactions on Networking*, 20(5):1466–1478, 2012.
- Han, S., Mao, H., and Dally, W. J. Deep compression: Compressing deep neural networks with pruning, trained quantization and huffman coding. *arXiv preprint arXiv:1510.00149*, 2015.
- He, K., Zhang, X., Ren, S., and Sun, J. Deep residual learning for image recognition. In *Proceedings of the IEEE Conference on Computer Vision and Pattern Recognition*, pp. 770–778. IEEE, 2016.
- Huang, H., Zhang, L., Sun, C., Fang, R., Yuan, X., and Wu, D. Distributed pruning towards tiny neural networks in federated learning. In *2023 IEEE 43rd International Conference on Distributed Computing Systems (ICDCS)*, pp. 190–201. IEEE, 2023.
- Huang, H., Zhuang, W., Chen, C., and Lyu, L. Fedmef: Towards memory-efficient federated dynamic pruning. In *Proceedings of the IEEE/CVF Conference on Computer Vision and Pattern Recognition*, pp. 27548–27557, 2024.
- Janowsky, S. A. Pruning versus clipping in neural networks. *Physical Review A*, 39(12):6600, 1989.
- Jayakumar, S., Pascanu, R., Rae, J., Osindero, S., and Elsen, E. Top-kast: Top-k always sparse training. *Advances in Neural Information Processing Systems*, 33:20744–20754, 2020.
- Jiang, Y., Wang, S., Valls, V., Ko, B. J., Lee, W.-H., Leung, K. K., and Tassiulas, L. Model pruning enables efficient federated learning on edge devices. *IEEE Transactions on Neural Networks and Learning Systems*, 34(12):10374–10386, 2022.
- Kairouz, P., McMahan, H. B., Avent, B., Bellet, A., Bennis, M., Bhagoji, A. N., Bonawitz, K., Charles, Z., Cormode, G., Cummings, R., et al. Advances and open problems in federated learning. *Foundations and trends® in machine learning*, 14(1–2):1–210, 2021.
- Komiyama, J., Honda, J., and Nakagawa, H. Optimal regret analysis of thompson sampling in stochastic multi-armed bandit problem with multiple plays. In *International Conference on Machine Learning*, pp. 1152–1161. PMLR, 2015.
- Kong, F., Yang, Y., Chen, W., and Li, S. The hardness analysis of thompson sampling for combinatorial semi-bandits with greedy oracle. *Advances in Neural Information Processing Systems*, 34:26701–26713, 2021.
- Krizhevsky, A., Hinton, G., and et al. Learning multiple layers of features from tiny images. In *Proceedings of the International Conference on Machine Learning*. PMLR, 2009.
- LeCun, Y., Denker, J., and Solla, S. Optimal brain damage. *Advances in neural information processing systems*, 2, 1989.
- Lee, N., Ajanthan, T., and Torr, P. Snip: Single-shot network pruning based on connection sensitivity. In *International Conference on Learning Representations*, 2018.
- Li, H., Kadav, A., Durdanovic, I., Samet, H., and Graf, H. P. Pruning filters for efficient convnets. *arXiv preprint arXiv:1608.08710*, 2016.

- Li, X., Huang, K., Yang, W., Wang, S., and Zhang, Z. On the convergence of fedavg on non-iid data. *arXiv preprint arXiv:1907.02189*, 2019.
- Louizos, C., Welling, M., and Kingma, D. P. Learning sparse neural networks through l_0 regularization. In *International Conference on Learning Representations*, 2018.
- Ma, X., Qin, M., Sun, F., Hou, Z., Yuan, K., Xu, Y., Wang, Y., Chen, Y.-K., Jin, R., and Xie, Y. Effective model sparsification by scheduled grow-and-prune methods. *arXiv preprint arXiv:2106.09857*, 2021.
- McMahan, B., Moore, E., Ramage, D., Hampson, S., and y Arcas, B. A. Communication-efficient learning of deep networks from decentralized data. In *Artificial intelligence and statistics*, pp. 1273–1282. PMLR, 2017.
- Mocanu, D. C., Mocanu, E., Stone, P., Nguyen, P. H., Gibescu, M., and Liotta, A. Scalable training of artificial neural networks with adaptive sparse connectivity inspired by network science. *Nature communications*, 9 (1):1–12, 2018.
- Molchanov, P., Mallya, A., Tyree, S., Frosio, I., and Kautz, J. Importance estimation for neural network pruning. In *Proceedings of the IEEE/CVF conference on computer vision and pattern recognition*, pp. 11264–11272, 2019a.
- Molchanov, P., Tyree, S., Karras, T., Aila, T., and Kautz, J. Pruning convolutional neural networks for resource efficient inference. In *5th International Conference on Learning Representations, ICLR 2017-Conference Track Proceedings*, 2019b.
- Mozer, M. C. and Smolensky, P. Skeletonization: A technique for trimming the fat from a network via relevance assessment. *Advances in neural information processing systems*, 1, 1988.
- Munir, M. T., Saeed, M. M., Ali, M., Qazi, Z. A., and Qazi, I. A. Fedprune: Towards inclusive federated learning. *arXiv preprint arXiv:2110.14205*, 2021.
- Netzer, Y., Wang, T., Coates, A., Bissacco, A., Wu, B., and Ng, A. Y. Reading digits in natural images with unsupervised feature learning. In *Proceedings of the 2011 Neural Information Processing Systems (NIPS)*, 2011.
- Perrault, P., Boursier, E., Valko, M., and Perchet, V. Statistical efficiency of thompson sampling for combinatorial semi-bandits. *Advances in Neural Information Processing Systems*, 33:5429–5440, 2020.
- Phillips, J. M. Chernoff-hoeffding inequality and applications. *arXiv preprint arXiv:1209.6396*, 2012.
- Qiu, X., Fernandez-Marques, J., Gusmao, P. P., Gao, Y., Parcollet, T., and Lane, N. D. ZeroFl: Efficient on-device training for federated learning with local sparsity. *arXiv preprint arXiv:2208.02507*, 2022.
- Raihan, M. A. and Aamodt, T. Sparse weight activation training. *Advances in Neural Information Processing Systems*, 33:15625–15638, 2020.
- Reddi, S., Charles, Z., Zaheer, M., Garrett, Z., Rush, K., Konečný, J., Kumar, S., and McMahan, H. B. Adaptive federated optimization. *arXiv preprint arXiv:2003.00295*, 2020.
- Singh, S. P. and Alistarh, D. Woodfisher: Efficient second-order approximation for neural network compression. *Advances in Neural Information Processing Systems*, 33: 18098–18109, 2020.
- Slivkins, A. et al. Introduction to multi-armed bandits. *Foundations and Trends® in Machine Learning*, 12(1-2):1–286, 2019.
- Tanaka, H., Kunin, D., Yamins, D. L., and Ganguli, S. Pruning neural networks without any data by iteratively conserving synaptic flow. *Advances in Neural Information Processing Systems*, 33:6377–6389, 2020.
- Tian, C. X., Liu, Y., Li, H., Cheung, R. C., and Wang, S. Gradient-congruity guided federated sparse training. *arXiv preprint arXiv:2405.01189*, 2024.
- Wang, Q. and Chen, W. Improving regret bounds for combinatorial semi-bandits with probabilistically triggered arms and its applications. *Advances in Neural Information Processing Systems*, 30, 2017.
- Wang, S. and Chen, W. Thompson sampling for combinatorial semi-bandits. In *International Conference on Machine Learning*, pp. 5114–5122. PMLR, 2018.
- Yu, R., Li, A., Chen, C.-F., Lai, J.-H., Morariu, V. I., Han, X., Gao, M., Lin, C.-Y., and Davis, L. S. Nisp: Pruning networks using neuron importance score propagation. In *Proceedings of the IEEE conference on computer vision and pattern recognition*, pp. 9194–9203, 2018.
- Zhang, X., Zhou, X., Lin, M., and Sun, J. Shufflenet: An extremely efficient convolutional neural network for mobile devices. In *Proceedings of the IEEE conference on computer vision and pattern recognition*, pp. 6848–6856, 2018.

A. Related Work

A.1. Neural Network Pruning

Neural network pruning (Mozer & Smolensky, 1988; LeCun et al., 1989; Janowsky, 1989) optimizes network structures by removing redundant components like connections (Han et al., 2015), neurons (Yu et al., 2018), or filters (Li et al., 2016). Traditional pruning methods focus on inference, requiring dense training followed by importance-based pruning and retraining. These importance scores are derived from weight magnitudes (Janowsky, 1989; Han et al., 2015), gradients (Mozer & Smolensky, 1988; Molchanov et al., 2019b), Fisher information (Singh & Alistarh, 2020), and other variants (Louizos et al., 2018; Yu et al., 2018). However, training a dense model first increases computational and memory costs.

Therefore, Recent works propose dynamic sparse training (Mocanu et al., 2018; Dettmers & Zettlemoyer, 2019; Evci et al., 2020) to bypass the dense training by iteratively adjusting sparse topologies during training while maintaining a fixed model size. Yet, existing methods rely on deterministic adjustments, leading to high variance and resource-intensive searches, exacerbated in federated learning under data heterogeneity and partial client availability. To address this, we propose TSAdj, which employs probabilistic adjustments for a more robust and stable model topology.

A.2. Federated Pruning

Federated Pruning is a technique that applies neural network pruning within the Federated Learning (FL) process. To avoid the requirements of dense training in traditional pruning methods, some previous methods determine the sparse model topology before federated training and do not adjust it during the FL process, such as SNIP (Lee et al., 2018) and Synflow (Tanaka et al., 2020). This approach of pruning at initialization may overlook crucial data information, potentially leading to suboptimal model structures.

Dynamic sparse training methods, such as those employed by PruneFL (Jiang et al., 2022), adjust the model during FL rounds. However, these methods require the entire model gradient to be sent to the server to ensure final performance, resulting in high communication costs. FedDST (Bibikar et al., 2022) and FedSGC (Tian et al., 2024) alleviate this issue by applying dynamic sparse training on clients. FedTiny (Huang et al., 2023) and FedMef (Huang et al., 2024) require clients only to upload the Top gradients. Despite these advancements, these methods adjust the model topology based on limited information from the currently selected clients, leading to issues of greedy adjustment and unstable topology. FedRTS addresses these challenges by applying TSAdj, significantly mitigating the problems associated with limited client information and enhancing the

robustness of model adjustments by leveraging probabilistic distributions.

A.3. Combinatorial Multi-Arm Bandit

The Combinatorial Multi-Armed Bandit (CMAB) problem extends the classical MAB to combinatorial settings, where rewards depend on selected arm combinations. (Gai et al., 2012) introduced the CMAB framework with linear rewards and proposed a UCB-type algorithm that allows approximation oracles for decision-making. This work established the foundation for CMAB analysis. (Chen et al., 2013; 2016) and (Wang & Chen, 2017) generalized the CMAB framework by introducing probabilistically triggered arms and relaxing reward assumptions to monotonicity. They proposed the CUCB algorithm, achieving regret bounds with approximation oracles and enabling broader applications of CMAB.

Despite these advancements, UCB-based algorithms, such as CUCB, rely on assumptions like monotonicity for reward functions. However, these assumptions may not hold in more complex scenarios, such as non-monotonic rewards or high-dimensional combinatorial action spaces. (Wang & Chen, 2018) pointed out that these limitations restrict the practicality of UCB algorithms, particularly in settings where reward functions are highly nonlinear or lack smoothness.

Thompson Sampling (TS) offers greater flexibility by avoiding monotonicity. TS has been shown to achieve regret bounds comparable to CUCB, as demonstrated by (Komiya et al., 2015) and (Wang & Chen, 2018), while (Perrault et al., 2020) further improved its performance coefficients. (Kong et al., 2021) extended the theoretical understanding of CMAB by conducting a detailed hardness analysis on regret and bounds when using greedy oracles. Their study quantified the impact of greedy oracles on regret and provided analytical results for scenarios where exact solutions are unavailable. Additionally, their analysis addressed the convergence of TS in combinatorial settings, highlighting its robustness in handling complex reward structures.

B. Algorithm

B.1. TSAdj

In each loop t , the aggregated weights W_{t+1}^{agg} will be calculated in each loop when the server receives the weights W_{t+1}^n from each client $n \in C_t$, and TSAdj is invoked to adjust the sparse topology m_t only in the outer loop. The outcomes $X_{t,i}$ for link m_i are computed as described in Equation 3, which balances global and client-specific contributions. Specifically, outcomes $X_{t,i}^{agg}$ and $X_{t,i}^n$ are calculated based on Equations 4 and 5 on the server, using the

aggregated weights W_{t+1} and the uploaded weights W_{t+1}^n , while $X_{t,i}^n$ will be updated in the outer loop using the indices of the top $K - \kappa$ gradients \mathcal{I}_{t+1}^n from each client n based on Equation 6. Outcomes $X_{t,i}^{agg}$ and $X_{t,i}^n$ are combined to compute the final outcome $X_{t,i}$ for link m_i in Equation 3, where $\gamma \in [0, 1]$ controls the trade-off between global and client-specific contributions, and p_n reflects the relative weight of client n based on the size of its local dataset D_n . A larger γ emphasizes client-specific observations, while a smaller γ prioritizes global contributions.

The prior probability distribution P for each link m_i in the topology m is modeled as a beta distribution parameterized by (α_i, β_i) . At initialization, (α_i, β_i) are set to small positive values (e.g., $\alpha_i = \beta_i = 1$) to represent a uniform prior, ensuring that all links have an equal probability of activation at the outset. The beta parameters (α_i, β_i) for each link m_i are then updated incorporating with the computed outcomes $X_{t,i}$, via Equation 7, where λ controls the trade-off between exploration and exploitation by adjusting the impact of the current outcomes on the beta distribution's update. A larger λ increases the influence of the current loop's outcomes $X_{t,i}$, accelerating the concentration of the Beta distribution towards a certain probability. Conversely, a smaller λ preserves uncertainty to encourage exploration. Over time, as α_i and β_i grow under the influence of λ and $X_{t,i}$, the Beta distribution becomes sharper and more concentrated, reflecting an increasingly certain probability of selecting m_i as an active link in the topology m .

In each loop t , the topology adjustment dynamically activates or deactivates links based on a probabilistic action S_t in Equation 2, where ξ is sampled from the updated posterior distribution P . For each link m_i , the probability ξ_i is independently sampled from its corresponding Beta distribution P_i . Links are activated if their probabilities ξ_i rank among the top K in magnitude. The TSAAdj mechanism outputs the updated sparse topology m_{t+1} and the weights $W_{t+1} \odot m_{t+1}$, where \odot denotes element-wise multiplication. The updated mask m_{t+1} represents the optimized topology for the next training loop $t + 1$.

B.2. FedRTS

The framework of FedRTS begins by initializing the global model weights W_0 and a sparse mask m_0 with a predefined sparsity level d' . The sparse mask m_0 determines the active parameters in the initial global model. Additionally, hyperparameters such as the total number of training loops T_{end} and the adjustment interval ΔT are set. These parameters control the frequency of topology adjustments and the overall training duration.

The training process is conducted over T_{end} loops. At the beginning of each training loop t , the server employs a random sampling mechanism to select a subset of clients

C_t from the total \mathcal{N} available clients for participation in the training process. This sampling process is conducted uniformly at random, ensuring that each client, indexed by n from $1, \dots, \mathcal{N}$, has an equal probability of being chosen. This randomized partial participation mechanism not only avoids bias in client selection but also ensures scalability and reduces communication overhead, making it well-suited for large-scale distributed systems.

Algorithm 2 FedRTS

Input: Initial model W_0 , sparsity d' , total loops T_{end} , adjustment interval ΔT
Output: Final sparse model $W_{T_{end}}, m_{T_{end}}$
 Randomly initialize m_0 with sparsity d' ,
for each loop $t=0, 1, 2, \dots, T_{end} - 1$ **do**
 Sample a random subset of clients C_t
 Broadcast server model (W_t, m_t) to all clients $n \in C_t$
 for each client $n \in C_t$ **do**
 Receive model W_t and mask m_t from the server
 $W_{t+1}^n \leftarrow$ perform local training on D_n
 Transmit W_{t+1}^n to server
 if $t \bmod \Delta T = 0$ and $t < T_{end}$ **then**
 Compute gradients G_{t+1}^n respect to loss function
 $\mathcal{I}_{t+1}^n \leftarrow \{i | i \in \text{Top}(|G_{t+1}^n|, K - \kappa)\}$
 Transmit \mathcal{I}_{t+1}^n to server
 end if
 end for
 The server does
 if $t \bmod \Delta T = 0$ and $t < T_{end}$ **then**
 $W_{t+1}^{agg}, m_{t+1} = \text{TSAAdj}(\{W_{t+1}^n, \mathcal{I}_{t+1}^n | n \in C_t\})$
 else
 $W_{t+1}^{agg} \leftarrow \sum_{n \in C_t} p_n W_{t+1}^n$
 $m_{t+1} \leftarrow m_t$
 $X_t^{agg} \leftarrow$ calculated by Eq.4 based on W_{t+1}^{agg}
 $X_t^n \leftarrow$ calculated by Eq.5 based on W_{t+1}^n
 $X_t \leftarrow (1 - \gamma)X_t^{agg} + \gamma \sum_{n \in C_{t+1}} p_n X_t^n$
 $(\alpha_i, \beta_i) \leftarrow (\alpha_i + \lambda X_{t,i}, \beta_i + \lambda(1 - X_{t,i}))$, $X_{t,i} \neq \text{None}$
 end if
end for

The server then broadcasts the global sparse weights W_t and the corresponding mask m_t to all participating clients C_t . Each selected client $n \in C_t$ trains the received model (W_t, m_t) on its local dataset D_n for a fixed number of loops, producing intermediate outputs. Specifically, gradients G_{t+1}^n will be computed only during outer loops for topology adjustment. The client identifies the gradients with the top $K - \kappa$ magnitudes based on the gradients G_{t+1}^n and upload its corresponding indices $\mathcal{I}_{t+1}^n = \{i | i \in \text{Top}(|G_{t+1}^n|, K - \kappa)\}$, representing the most promising links for the potential reactivation, rather than the complete gradients to the server, further reducing communication overhead. In contrast, weights W_{t+1}^n are computed and uploaded to the

server during both inner and outer loops to facilitate global aggregation. Unlike gradients, which are selectively uploaded, the complete set of weights is transmitted to ensure comprehensive integration into the global model.

Upon receiving the locally updated gradient indices \mathcal{I}_{t+1}^n in the outer loop and weights W_{t+1}^n from the participating clients, the server aggregates the weights to update global model weights W_{t+1}^n using a weighted average formula. Mathematically, the aggregated weights W_{t+1}^{agg} are computed as: $W_{t+1}^{agg} = \sum_{n \in C_t} p_n W_{t+1}^n$. If the current loop t is an outer loop (i.e., $t \bmod \Delta T = 0$), the server invokes the TSAdj mechanism to adjust the sparse mask m_t . The updated mask m_{t+1} is then applied to the global model.

After completing T_{end} training loops, the server outputs the final globally aggregated weights $W_{T_{end}}$ and an optimized mask $m_{T_{end}}$, both derived from the iterative training involving all participating clients. The weights $W_{T_{end}}$ represent the learned parameters that effectively accommodate heterogeneous data distributions, while the topology $m_{T_{end}}$ preserves the robust and reliable structure of the model.

C. Theoretical Details

C.1. Greedy Optimal Action

Algorithm 3 Greedy Optimal Action

Input: The mean vector μ and action size K

Return: The greedy optimal action S^*

Initialize: $S^* = \emptyset$

for $k \in 1, \dots, K$ **do**

$S^* = S^* \cup \{\arg\max_{i \notin S^*} r(S^* \cup \{i\}, \mu)\}$

end for

C.2. Proof of Theorem 3.4

The cumulative regret $Reg(T)$ is defined as:

$$Reg(T) = \mathbb{E} \left[\sum_{t=1}^T \Delta_{S_t} \right], \quad (11)$$

where $\Delta_{S_t} = \max\{r(S^*, \mu) - r(S_t, \mu), 0\}$ and S^* is the greedy optimal action based on μ , which is obtained by Alg. 3. The maximum reward gap is set as $\Delta_{\max} = \max_S \Delta_S$. The maximum reward gap of actions containing arm s is $\Delta_s^{\max} = \max_{S: s \in S} \Delta_S$. We define S^* and S_t are sequences, i.e., $S^* = (s_1^*, \dots, s_K^*)$, $S_t = (s_{t,1}, \dots, s_{t,K})$, and $s_k^* \in S^*$ is the k -th element added to S^* . We denote $S_k^* = (s_1^*, \dots, s_k^*)$ and $S_{t,k} = (s_{t,1}, \dots, s_{t,k})$. For any arm s , define the marginal reward gap $\Delta_{s,k} = r(S_k^*, \mu) - r(S_{k-1}^* \cup \{s\}, \mu)$.

Theorem. (Upper Bound) Under assumptions 3.1, 3.2 and 3.3 and with outcomes defined in Eq. 8, the regret

$Reg(T)$ of TSAdj can be upper bounded by:

$$\begin{aligned} Reg(T) &\leq \sum_{s \neq s_1^*} \max_{k: s \notin S_k^*} \frac{6\Delta_s^{\max} L^2 \log T}{(\Delta_{s,k} - 2BK\epsilon)^2} \\ &\quad + \left(2K + 4\langle W \rangle + \frac{KU + 8K\epsilon^4}{\epsilon^6} \right) \Delta_{\max} \quad (12) \\ &= O \left(\sum_{s \neq s_1^*} \max_{k: s \notin S_k^*} \frac{\Delta_{\max} L^2 \log T}{\Delta_{s,k}^2} \right). \end{aligned}$$

for any ϵ such that $\forall s \neq s_1^*$ and $i \notin S_k^*$, $\Delta_{s,k} > 2BK\epsilon$, where U is a universal constant.

Proof. Our proof follows (Kong et al., 2021). For any arm $s \neq s_1^*$, we apply the exploration price $F(i)$ as

$$F(s) = \max_{k: s \notin S_k^*} \frac{6L^2 \log T}{(\Delta_{s,k} - 2LK\epsilon)^2} \quad (13)$$

Therefore, at t -th iteration, there are two event

$$A_t := \left\{ \exists i \in \{1, \dots, \langle W \rangle\} \Rightarrow |\xi_{t,i} - \hat{\mu}_{t,i}|^2 > \frac{3 \log T}{2N_{t,i}} \right\} \quad (14)$$

$$B_t := \left\{ \exists i \in \{1, \dots, \langle W \rangle\} \Rightarrow |\mu_i - \hat{\mu}_{t,i}|^2 > \frac{3 \log T}{2N_{t,i}} \right\}, \quad (15)$$

where $N_{t,s} = \sum_{\tau=1}^t \mathbf{1}_{s \in S_\tau}$ is the number of observations of arm s and $\hat{\mu}_{t,s} = \frac{1}{N_{t,s}} \sum_{\tau=1}^t \sum_{s \in S_\tau} X_{\tau,s}$ is the empirical mean outcome of s at the start of round t .

Based on Eq. 14 and 15, the regret $Reg(T)$ can be divided into three terms as

$$\begin{aligned} Reg(T) &\leq \mathbb{E} \left[\sum_{t=1}^T \mathbf{1}_{\neg A_t \wedge \neg B_t} \Delta_{S_t} \right] + \mathbb{E} \left[\sum_{t=1}^T \mathbf{1}_{A_t} \Delta_{S_t} \right] \\ &\quad + \mathbb{E} \left[\sum_{t=1}^T \mathbf{1}_{B_t} \Delta_{S_t} \right]. \end{aligned} \quad (16)$$

We provide the Lemma C.1, C.2 and C.3 to bound these three terms one by one. Therefore, we can obtain

$$\begin{aligned} Reg(T) &\leq \sum_{s \neq s_1^*} \max_{k: s \notin S_k^*} \frac{6\Delta_s^{\max} L^2 \log T}{(\Delta_{s,k} - 2BK\epsilon)^2} \\ &\quad + \left(2K + 4\langle W \rangle + \frac{KU + 8K\epsilon^4}{\epsilon^6} \right) \Delta_{\max} \end{aligned} \quad (17)$$

Lemma C.1. Under all assumptions and settings in Theo-

rem 3.4, we have

$$\begin{aligned} \mathbb{E} \left[\sum_{t=1}^T \mathbf{1}_{\neg A_t \wedge \neg B_t} \Delta_{S_t} \right] &\leq \sum_{s \neq s_1^*} \max_{k: s \notin S_k^*} \frac{6\Delta_s^{\max} L^2 \log T}{(\Delta_{s,k} - 2BK\epsilon)^2} \\ &\quad + \left(2K + \frac{KU + 8K\epsilon^4}{\epsilon^6} \right) \Delta_{\max} \end{aligned} \quad (18)$$

Proof. To bound this term, we should study the difference between $s_{t,k}$ and s_k^* , that is, this term can be bounded by

$$\begin{aligned} \mathbb{E} \left[\sum_{t=1}^T \mathbf{1}_{\neg A_t \wedge \neg B_t} \Delta_{S_t} \right] &\leq \sum_{k=1}^K \mathbb{E} \left[\sum_{t=1}^T \Delta_{S_t} \cdot \mathbf{1}_{\neg A_t \wedge \neg B_t \wedge C_{t,k}} \right] \\ &\quad + \sum_{k=1}^K \mathbb{E} \left[\sum_{t=1}^T \mathbf{1}_{s_k^* = s_{t,k} \wedge \|\xi_{t,s_k^*} - \mu_{s_k^*}\|_\infty \leq \epsilon} \right] \cdot \Delta_{\max}, \end{aligned} \quad (19)$$

where $C_{t,k}$ denotes as an event which is defined as

$$C_{t,k} := \{s_{k-1}^* = S_{t,k-1} \wedge s_k^* \neq s_{t,k} \wedge \|\xi_{t,s_k^*} - \mu_{s_k^*}\|_\infty \leq \epsilon\}. \quad (20)$$

We define $\xi_{t,S} = \{\xi_{t,i} | i \in S\}$ and $\mu_S = \{\mu_i | i \in S\}$. According to Lemma C.4, the first term in Eq. 19 can be bounded by:

$$\begin{aligned} &\sum_{k=1}^K \mathbb{E} \left[\sum_{t=1}^T \Delta_{S_t} \cdot \mathbf{1}_{\neg A_t \wedge \neg B_t \wedge C_{t,k}} \right] \\ &\leq \sum_{k=1}^K \mathbb{E} \left[\sum_{s \notin S_k^*} \sum_{t=1}^T \Delta_{S_t} \cdot \mathbf{1}_{s=s_{t,k} \wedge N_{t,s} \leq F(s)} \right] + \frac{UK}{\epsilon^6} \Delta_{\max} \\ &\leq \mathbb{E} \left[\sum_{s \neq s_1^*} \sum_{t=1}^T \sum_{k=1}^K \Delta_{S_t} \cdot \mathbf{1}_{s=s_{t,k} \wedge N_{t,s} \leq F(s)} \right] + \frac{UK}{\epsilon^6} \Delta_{\max} \\ &\leq \mathbb{E} \left[\sum_{s \neq s_1^*} \sum_{t=1}^T \Delta_{S_t} \cdot \mathbf{1}_{s \in S_t \wedge N_{t,s} \leq F(s)} \right] + \frac{UK}{\epsilon^6} \Delta_{\max} \\ &\leq \sum_{s \neq s_1^*} F(s) \Delta_s^{\max} + \frac{UK}{\epsilon^6} \Delta_{\max} \\ &\leq \sum_{s \neq s_1^*} \max_{k: s \notin S_k^*} \frac{6\Delta_s^{\max} L^2 \log T}{(\Delta_{s,k} - 2BK\epsilon)^2} + \frac{UK}{\epsilon^6} \Delta_{\max}, \end{aligned} \quad (21)$$

where U is a universal constant. Based on Lemma C.5, the second term can be bounded by

$$\begin{aligned} &\sum_{k=1}^K \mathbb{E} \left[\sum_{t=1}^T \mathbf{1}_{s_k^* = s_{t,k} \wedge \|\xi_{t,s_k^*} - \mu_{s_k^*}\|_\infty \leq \epsilon} \right] \Delta_{\max} \\ &\leq 2K + \frac{8K}{\epsilon^2} \Delta_{\max}. \end{aligned} \quad (22)$$

Combining Eq. 21 and Eq. 22, we have

$$\begin{aligned} \mathbb{E} \left[\sum_{t=1}^T \mathbf{1}_{\neg A_t \wedge \neg B_t} \Delta_{S_t} \right] &\leq \sum_{s \neq s_1^*} \max_{k: s \notin S_k^*} \frac{6\Delta_s^{\max} L^2 \log T}{(\Delta_{s,k} - 2BK\epsilon)^2} \\ &\quad + \left(2K + \frac{KU + 8K\epsilon^4}{\epsilon^6} \right) \Delta_{\max}. \end{aligned} \quad (23)$$

Lemma C.2. Under all assumptions and setting in Theorem 3.4, we have

$$\mathbb{E} \left[\sum_{t=1}^T \mathbf{1}_{A_t} \Delta_{S_t} \right] \leq 2\Delta_{\max} \langle W \rangle. \quad (24)$$

Proof.

$$\begin{aligned} \mathbb{E} \left[\sum_{t=1}^T \mathbf{1}_{A_t} \Delta_{S_t} \right] &\leq \mathbb{E} \left[\sum_{t=1}^T \mathbf{1}_{A_t} \right] \Delta_{\max} \\ &\leq \sum_{i=1}^{\langle W \rangle} \mathbb{E} \left[\sum_{t=1}^T \mathbf{1}_{|\xi_{t,i} - \hat{\mu}_{t,i}|^2 > \frac{3 \log T}{2N_{t,i}}} \right] \Delta_{\max} \\ &\leq \sum_{i=1}^{\langle W \rangle} \sum_{t=1}^T \sum_{\tau=1}^{T-1} \mathbb{P} \left(N_{t,i} = \tau \wedge |\xi_{t,i} - \hat{\mu}_{t,i}|^2 > \frac{3 \log T}{2N_{t,i}} \right) \Delta_{\max} \\ &= \sum_{i=1}^{\langle W \rangle} \sum_{t=1}^T \sum_{\tau=1}^{T-1} \mathbb{P}(N_{t,i} = \tau) \\ &\quad \cdot \mathbb{P} \left(|\xi_{t,i} - \hat{\mu}_{t,i}|^2 > \frac{3 \log T}{2N_{t,i}} \middle| N_{t,i} = \tau \right) \Delta_{\max}. \end{aligned} \quad (25)$$

According to Lemma C.6, we have

$$\begin{aligned} &\sum_{i=1}^{\langle W \rangle} \sum_{t=1}^T \sum_{\tau=1}^{T-1} \mathbb{P}(N_{t,i} = \tau) \\ &\quad \cdot \mathbb{P} \left(|\xi_{t,i} - \hat{\mu}_{t,i}|^2 > \frac{3 \log T}{2N_{t,i}} \middle| N_{t,i} = \tau \right) \Delta_{\max} \\ &\leq \sum_{i=1}^{\langle W \rangle} \sum_{t=1}^T \sum_{\tau=1}^{T-1} \mathbb{P}(N_{t,i} = \tau) \cdot 2 \exp(-3 \log T) \Delta_{\max} \\ &\leq \sum_{i=1}^{\langle W \rangle} \sum_{t=1}^T \frac{2}{T} \Delta_{\max} \\ &= 2\Delta_{\max} \langle W \rangle. \end{aligned} \quad (26)$$

Lemma C.3. With all assumptions and setting in Theorem 3.4, we have

$$\mathbb{E} \left[\sum_{t=1}^T \mathbf{1}_{B_t} \Delta_{S_t} \right] \leq 2\Delta_{\max} \langle W \rangle. \quad (27)$$

Proof.

$$\begin{aligned}
 \mathbb{E} \left[\sum_{t=1}^T \mathbf{1}_{B_t} \Delta_{S_t} \right] &\leq \mathbb{E} \left[\sum_{t=1}^T \mathbf{1}_{B_t} \right] \Delta_{\max} \\
 &\leq \sum_{i=1}^{\langle W \rangle} \mathbb{E} \left[\sum_{t=1}^T \mathbf{1}_{|\mu_i - \hat{\mu}_{t,i}|^2 > \frac{3 \log T}{2N_{t,i}}} \right] \Delta_{\max} \\
 &\leq \sum_{i=1}^{\langle W \rangle} \sum_{t=1}^T \sum_{\tau=1}^{T-1} \mathbb{P} \left(N_{t,i} = \tau \wedge |\mu_i - \hat{\mu}_{t,i}|^2 > \frac{3 \log T}{2N_{t,i}} \right) \Delta_{\max} \\
 &= \sum_{i=1}^{\langle W \rangle} \sum_{t=1}^T \sum_{\tau=1}^{T-1} \mathbb{P}(N_{t,i} = \tau) \\
 &\quad \cdot \mathbb{P} \left(|\mu_i - \hat{\mu}_{t,i}|^2 > \frac{3 \log T}{2N_{t,i}} \middle| N_{t,i} = \tau \right) \Delta_{\max}.
 \end{aligned} \tag{28}$$

According to Lemma C.7, we have

$$\begin{aligned}
 &\sum_{i=1}^{\langle W \rangle} \sum_{t=1}^T \sum_{\tau=1}^{T-1} \mathbb{P}(N_{t,i} = \tau) \\
 &\quad \cdot \mathbb{P} \left(|\mu_i - \hat{\mu}_{t,i}|^2 > \frac{3 \log T}{2N_{t,i}} \middle| N_{t,i} = \tau \right) \Delta_{\max} \\
 &\leq \sum_{i=1}^{\langle W \rangle} \sum_{t=1}^T \sum_{\tau=1}^{T-1} \mathbb{P}(N_{t,i} = \tau) \cdot 2 \exp(-3 \log T) \Delta_{\max} \\
 &\leq \sum_{i=1}^{\langle W \rangle} \sum_{t=1}^T \frac{2}{T} \Delta_{\max} \\
 &= 2 \Delta_{\max} \langle W \rangle.
 \end{aligned} \tag{29}$$

Lemma C.4. Under all assumptions and settings in Theorem 3.4, with $C_{t,k}$ defined in Eq. 20, we have

$$\begin{aligned}
 &\mathbb{E} \left[\sum_{t=1}^T \Delta_{S_t} \cdot \mathbf{1}_{\neg A_t \wedge \neg B_t \wedge C_{t,k}} \right] \\
 &\leq \mathbb{E} \left[\sum_{s \notin S_k^*} \sum_{t=1}^T \Delta_{S_t} \cdot \mathbf{1}_{s=s_{t,k} \wedge N_{t,s} \leq F(s)} \right] + \frac{U \Delta_{\max}}{\epsilon^6}.
 \end{aligned} \tag{30}$$

Proof. This Lemma is a special case in (Kong et al., 2021) (Lemma 1), setting the size of unit as 1 and $U = CC'$.

Lemma C.5. With all assumptions and setting in Theorem 3.4, we have

$$\mathbb{E} \left[\sum_{t=1}^T \mathbf{1}_{s_k^* = s_{t,k} \wedge \|\xi_{t,s_k^*} - \mu_{s_k^*}\|_{\infty} \leq \epsilon} \right] \Delta_{\max} \leq 2 + \frac{8}{\epsilon^2} \Delta_{\max} \tag{31}$$

Proof. This Lemma is a special case in (Kong et al., 2021) (Lemma 3), setting the size of each unit as 1.

Lemma C.6. With all assumptions and setting in Theorem 3.4, for any arm $i \in \{1, \dots, \langle W \rangle\}$ and round t , we have

$$\mathbb{P}(|\xi_{t,i} - \hat{\mu}_{t,i}|^2 > \epsilon | \alpha_{t,i}, \beta_{t,i}) \leq 2 \exp(-2\epsilon N_{t,i}), \tag{32}$$

where $\alpha_{t,i}$ and $\beta_{t,i}$ are the values of α_t and β_t in the TSAAdj before the start of round t

Proof. This Lemma has been proved in (Wang & Chen, 2018) (Lemma 3).

Lemma C.7. With all assumptions and setting in Theorem 3.4, let X_1, \dots, X_K be identical independent random variable such that $X_i \in [0, 1]$ and $\mathbb{E}[X_i] = \mu$ for any $i \in \{1, \dots, K\}$. Then for any $\epsilon \geq 0$, we have

$$\mathbb{P} \left(\left| \sum_{i=1}^K X_i - \mu \right| > K\epsilon \right) \leq 2 \exp(-2K\epsilon^2), \tag{33}$$

Proof. This Lemma can be proved by Chernorff-Hoeffding Bound in (Phillips, 2012)(Theorem 1.1).

D. Additional Setup Details

This section provides supplementary information to the main contents, elaborating on the datasets, hyperparameter details, and baseline frameworks used in our experiments.

D.1. Datasets

In the CV tasks, we apply our approach using ResNet18 on CIFAR-10, CINIC-10 and SVHN datasets.

- **CIFAR-10:** It contains 50,000 training images and 10,000 testing images. Each image in CIFAR-10 is a 3×32×32 RGB image, implying 10 classes of objects.
- **CINIC-10:** It contains three equal subsets - train, validation, and test—each comprising 90,000 images. CINIC-10 is an extended version of CIFAR-10 that includes additional images from ImageNet.
- **SVHN:** There are 73,257 digit images in the training set and 26,032 images in the testing set. The digit images are obtained from house numbers in Google Street View images.

In the NLP tasks, we choose GPT-2-32M as the backbone model with the TinyStories dataset. TinyStories contains synthetically generated short stories that only use a limited vocabulary. We truncate each story to 256 tokens, with 2,120,000 stories used for training and 22,000 for testing.

D.2. Hyperparameter Details

In addition to the Federated Learning settings described earlier, we provide more detailed hyperparameter configurations. In the TSAAdj, we define $\kappa = 0.2 \left(4 - \cos \frac{t\pi}{T_{end}} \right) K^l$ at t -th loop, where K^l represents the number of active parameters in l -th layer. The optimizer used is Adam, with a learning rate of $\eta = 0.001$. To generate non-iid data distributions on the client, we utilize the Dirichlet distribution. For CV tasks, we set the heterogeneity degree α to 0.5, which controls the distribution of labels among local datasets. In the NLP tasks, we apply the Dirichlet distribution to create data imbalance, setting α to 5.

D.3. Baselines

The selected federated pruning baselines differ in their approaches to sparse model initialization and subsequent model topology adjustment:

- **PruneFL**: Initializes the sparse model by training on a powerful device and applies adaptive pruning by importance measure. In our implementation, we perform random pruning instead of pruning with powerful devices due to resource constraints. Moreover, we set the time t_j of each parameter j with 1.
- **FedDST**: Applies dynamic sparse training on clients and performs greedy aggregation to produce a new global topology.
- **FedTiny**: Initializes the model by adaptive batch normalization selection and adjusts the model mask based on the aggregated top-K gradients of parameters. We disable the adaptive batch normalization selection due to high communication overhead.
- **FedSGC**: Adjusts model topology on devices guided by the gradient congruity, which is similar to FedDST but requires extra communication cost.
- **FedMef**: Utilizes budget-aware extrusion to transfer essential information of pruned parameters to other parameters and reduces activation memory by scaled activation pruning. In our experiment, we disable the scaled activation pruning due to computational overhead.

E. Additional Experiments Results

To further validate our findings, we perform additional experiments to investigate the impact of various hyperparameters and the convergence behavior of our proposed methods.

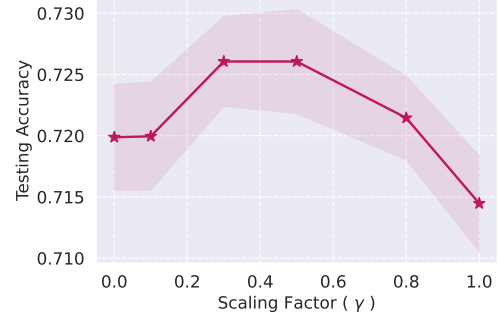


Figure 8. Impact of trade-off ratio γ

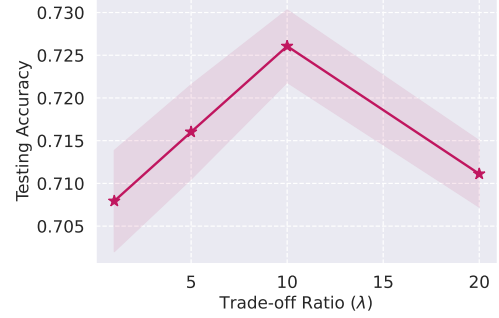


Figure 9. Impact of the scaling factor λ

E.1. Impact of trade-off ratio γ

The trade-off ratio γ modulates the weight of individual models' information. Traditional methods only incorporate the information from the aggregated model, which is insufficient. To verify the impact of individual models' information, we conduct experiments on the trade-off ratio γ . As illustrated in Fig. 8, the test accuracy reaches its peak when the γ value is between 0.3 and 0.5. This indicates that the information from both individual models and the aggregated model is significant in model topology adjustment. Consequently, the γ value is set to 0.5 in the main experiments.

E.2. Impact of the scaling factor λ

The scaling factor λ regulates the impact of the current reward $X(t)$ at step t . A λ value that is too small will amplify the uncertainty in Thompson Sampling, whereas a λ value that is too large will disregard the uncertainty arising from sample insufficiency. Thus, selecting an appropriate value for λ is crucial for enhancing FedRTS's performance. In a separate set of experiments, the influence of the reward scaling λ on the results is investigated. Fig. 9 demonstrates that the test accuracy attains its maximum at approximately 0.73 when λ is 10. This finding indicates that a λ value of 10 is a reasonable choice, and therefore, we adopt $\lambda = 10$ in our main experiments to ensure optimal accuracy.

Table 3. Performance under Different Adjustment Interval (ΔT)

ΔT	3	5	10	20
FedDST	0.664	0.683	0.723	0.716
FedMef	0.745	0.737	0.713	0.705
FedRTS	0.735	0.722	0.734	0.731

E.3. The Impact of Adjustment Interval

When considering federated dynamic sparse training methods, the timing of adjustments (ΔT) between rounds holds paramount importance. Striking the right balance in this interval is crucial—a lengthy interval may lead to sparse adjustments, hindering optimal topology discovery, while a short interval may result in inadequate training periods between adjustments. In cases where a method struggles to swiftly recuperate from information loss post-topology changes, it can lead to unreliable adjustments and subpar outcomes. Our evaluation of FedRTS on the CIFAR-10 dataset involved exploring various adjustment intervals ($\Delta T \in \{3, 5, 10, 20\}$). As depicted in Table 3, FedRTS consistently outperformed baseline methods across most intervals. Notably, FedRTS’s performance improved with shorter intervals, showcasing its adeptness in efficiently recuperating from information loss post-topology adjustments—a trait starkly contrasting with FedDST’s diminishing performance under similar conditions.

E.4. Convergence

To compare the convergence speed of our proposed FedRTS with other state-of-the-art (SOTA) methods, we conducted experiments on validation accuracy using the CIFAR-10 and CINIC-10 datasets, focusing on cumulative FLOPs and Cumulative Communication Cost during training. On the CIFAR-10 dataset, our proposed FedRTS demonstrated superior accuracy compared to other SOTA frameworks in terms of cumulative FLOPs throughout the entire training period, as depicted in Figure 10. On the CINIC-10 dataset, initially, our proposed FedRTS lagged behind FedDST at the start of training but later outperformed almost all other SOTA frameworks in terms of cumulative communication cost and cumulative FLOPs for the remainder of the training period, as illustrated in Figure 11 and Figure 12. Although FedAVG outperformed FedRTS on CINIC-10 within a certain range of cumulative communication costs (between 150 – 200GB), FedRTS surpassed it thereafter, showcasing excellent convergence speed.

In Figure 10, initially, there are no apparent differences in cumulative FLOPs between $0 - 3 \times 10^{15}$, but thereafter, FedRTS consistently outperforms all other methods. Between cumulative FLOPs of $11 - 13 \times 10^{15}$, FedMef briefly outperforms FedRTS, but beyond that point, FedRTS clearly surpasses all other methods. This pattern showcases the

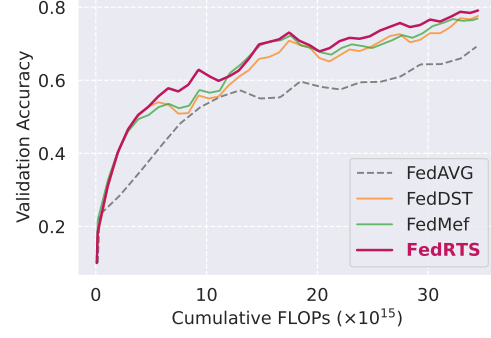


Figure 10. Validation accuracy of FedRTS and SOTA frameworks on CIFAR-10 dataset for cumulative FLOPs during training.

exceptional convergence speed of FedRTS in cumulative FLOPs on CIFAR-10.

In Figure 11, FedDST initially outperforms FedRTS and other methods within the range of cumulative communication costs between 10 – 50GB. However, FedRTS overtakes FedDST and other frameworks thereafter. When the cumulative communication cost exceeds 120GB, the validation accuracy of FedRTS experiences a temporary decline, resulting in lower performance than FedDST. Nonetheless, FedRTS surpasses FedDST once the cumulative communication cost surpasses 160GB. Notably, FedAVG outperforms all other methods between cumulative communication costs of 150 – 190GB but declines afterward. This phenomenon may stem from the stronger stability of FedAVG, allowing it to converge while other methods begin to fluctuate. Overall, Figure 11 highlights the outstanding convergence speed of FedRTS in cumulative communication costs on CINIC-10.

In Figure 12, FedDST initially surpasses FedRTS and other methods within the range of cumulative FLOPs between $1 - 15 \times 10^{15}$. However, FedRTS overtakes FedDST and outperforms other frameworks thereafter. Although FedDST outperforms FedRTS when cumulative FLOPs range between $35 - 44 \times 10^{15}$, FedRTS surpasses FedDST and other methods beyond that threshold. Overall, Figure 12 demonstrates the excellent convergence speed of FedRTS in cumulative FLOPs on CINIC-10.

F. Communication and Computational Cost

In our experiments, we analyzed the proposed FedRTS against other methods by examining the computational FLOPs and communication costs. We began by introducing sparse compression strategies and then detailed how we calculated these metrics.

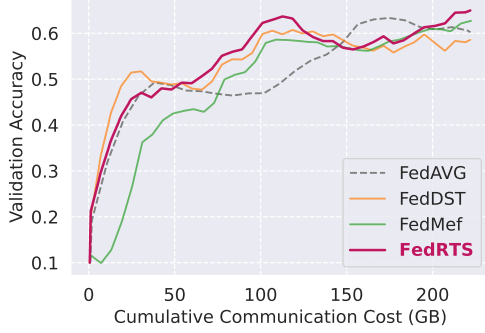


Figure 11. Validation accuracy of FedRTS and SOTA frameworks on CINIC-10 dataset for cumulative communicational cost during training.

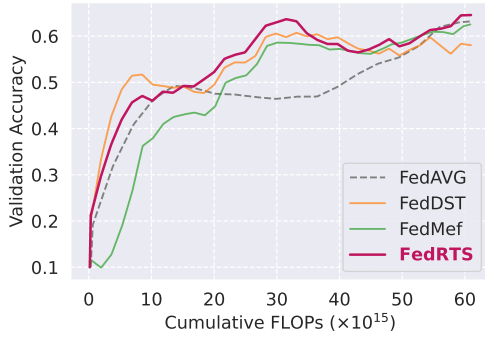


Figure 12. Validation accuracy of FedRTS and SOTA frameworks on CINIC-10 dataset for cumulative FLOPs during training.

F.1. Compression Strategy

When storing a matrix, two key components are values and positions. Compression techniques focus on reducing the storage required for the positions of non-zero values within the matrix. Consider a scenario where we aim to store the positions of m non-zero values with a b -bit width in a sparse matrix M , which comprises n elements and has a shape of $n_r \times n_c$. The density of the matrix, denoted by $d = m/n$, determines the compression scheme applied to represent M . The storage involves using o bits to represent the positions of the m non-zero values, resulting in an overall storage size of s .

- For density ($d \in [0.9, 1]$), a dense scheme is utilized, leading to $s = nb$.
- For density $d \in [0.3, 0.9)$, the bitmap (BM) method is employed, storing a map with n bits, where $o = n$ and $s = o + mb$.
- For density $d \in [0.1, 0.3)$, the coordinate offset (COO) scheme is applied, storing elements with their absolute offsets and requiring $o = m \lceil \log_2 n \rceil$ extra bits for

position storage. Thus, the overall storage becomes $s = o + mb$.

- For density $d \in [0., 0.1)$, the compressed sparse row (CSR) and compressed sparse column (CSC) methods are used based on size considerations. These methods use column and row indexes to store element positions, with CSR needing $o = m \lceil \log_2 n_c \rceil + n_r \lceil \log_2 m \rceil$ bits. The overall storage size is $s = o + mb$.

Reshaping is performed on tensors before compression, enabling the determination of the memory required for training the network’s parameters.

F.2. Communication Cost

In terms of communication costs, FedRTS shares a communication cost strategy similar to that of FedTiny. In contrast to other baseline methods like FedDST, where clients need to upload TopK gradients to the server every ΔR rounds to facilitate parameter expansion, the quantity of TopK gradients, denoted as ξ_t , aligns with the number of marked parameters θ low. Here, $\xi_t = \zeta_t(1 - s_m)n_\theta$, with $\zeta_t = 0.2(1 + \cos \frac{t\pi}{R_{stop}E})$ representing the adjustment rate for the t -th iteration. This results in minimal upload overhead. Moreover, there is no communication overhead for the model mask m during download since sparse storage formats like bitmap and coordinate offset contain the same element position information. Auxiliary data such as the learning rate schedule is excluded.

We define the storage for dense and sparse parameters as O_d and O_s respectively. Notably, in the inner loop, all federated pruning methods except FedAVG share the same communication cost, which amounts to $2O_s$. However, in the outer loop, different federated learning frameworks exhibit varying communication costs. The communication costs of different federated learning frameworks in the outer loop are detailed below:

- FedAVG: The data exchange amounts to $2O_d$, encompassing the uploading and downloading of dense parameters.
- FedDST: In this scenario, the model mask does not necessitate additional space for storage as the compressed sparse parameters already embody the mask information. Hence, the data exchange per round stands at $2O_s$, covering the upload and download of sparse parameters.
- PruneFL: PruneFL requires the clients to upload the full-size gradients squared for adjustment, therefore, the data exchange in the outer loop is $O_d + O_s$.
- FedSGC: FedSGC requires the server to send the gradient congruity to the server for each round, which has

the same size with sparse weight. Therefore, the data exchange in the outer loop is $3O_s$.

- FedTiny and FedMef: In comparison to FedDST, FedTiny and FedMef entail the upload of TopK gradients every ΔR rounds. Therefore, the maximum data exchange per round sums up to $2O_s + O_\xi$, where O_ξ signifies the storage required for the TopK gradients.
- FedRTS: When compared to FedTiny and FedMef, FedRTS only requires uploading the index of the TopK gradients every ΔR rounds, while FedTiny and FedMef necessitate uploading both the index and the values of TopK gradients at the same intervals. Consequently, the maximum data exchange per round amounts to $2O_s + 0.5O_\xi$, where O_ξ represents the storage needed for the TopK gradients.

F.3. Computational FLOPs

Training FLOPs encompass both forward-pass FLOPs and backward-pass FLOPs, with operations tallied on a per-layer basis. During the forward pass, layer activations are sequentially computed using prior activations and layer parameters. In the backward pass, each layer computes activation gradients and parameter gradients, with twice as many FLOPs expended in the backward pass as in the forward pass. FLOPs related to batch normalization and loss calculation are excluded.

In a detailed breakdown, assuming inference FLOPs for dense and static sparse models are denoted as F_d and F_s respectively, and the local iteration count is E , the maximum training FLOPs for each framework are as follows:

- FedAVG: Requires training a dense model, resulting in training FLOPs per round amounting to $3F_dE$.
- PruneFL: it requires calculating the dense gradients for each backward, therefore the training FLOPs is $(2F_d + F_s)E$.
- FedMef: Introduces a minor calculation overhead for BaE and SAP. Therefore, the maximum training FLOPs are estimated as $3(F_s + F_o)(E - 1) + (F_s + F_o) + 2F_d$, where F_o represents the computational overhead of BaE and SAP. F_o is approximated as $F_o = 4(1 - s_m)n_\theta + n_a \log n_a$, with $4(1 - s_m)n_\theta$ representing the FLOPs for regularization and WSCov, and $n_a \log n_a$ indicating the FLOPs for activation pruning.
- FedRTS, FedTiny, FedSGC, and FedDST: Implement RigL-based methods to adjust model architectures, necessitating clients to compute dense gradients in the final iteration. The maximum training FLOPs sum up to $3F_s(E - 1) + F_s + 2F_d$.